




Cite this: *Mater. Adv.*, 2024,  
5, 7609

Received 11th June 2024,  
Accepted 7th September 2024

DOI: 10.1039/d4ma00601a

rsc.li/materials-advances

## EDTA-functionalized hierarchical porous microspheres for effective cobalt ion recovery from water†

Mao-Hsuan Peng and Chia-Chen Li  \*

**The new adsorbent EDTA@PSV, which is a hierarchical porous microsphere modified with ethylenediaminetetraacetic acid, has demonstrated its effectiveness in extracting valuable metals. With a high surface area of 665 m<sup>2</sup> g<sup>−1</sup> and a large porosity of 90%, it exhibits significant potential for adsorbing Co<sup>2+</sup>, as supported by density functional theory simulations and experimental results.**

### Introduction

The sustainable utilization of valuable metals in industry is increasingly important due to metal resource scarcity and higher pollution levels. In order to promote a circular economy,<sup>1</sup> which emphasizes resource recovery and recycling rather than wasteful consumption, it is crucial to extract indestructible metal elements from waste. This way, we can innovate and create new materials that align with sustainable industrial practices. Several methods have been developed for removing or recovering valuable metal ions from wastewater. These include chemical precipitation,<sup>2</sup> chemical oxidation–reduction,<sup>3</sup> electrochemical treatment,<sup>4</sup> and adsorption.<sup>5,6</sup> Among these methods, adsorption is the most effective, as it generates less sludge and is more cost-effective than other techniques.

In the field of adsorption techniques, a wide range of adsorbents have been proposed, from activated carbon to metal–organic frameworks and polymers.<sup>7,8</sup> However, many of these materials struggle to achieve satisfactory adsorption capacities and rates. To address this issue, surface modification of adsorbents with ligands such as ethylene diamine tetraacetic acid (EDTA) has become increasingly popular.<sup>9,10</sup> EDTA possesses noteworthy chelating properties, thanks to its four carboxylic acids and two amine groups, which allow it to form

stable water-soluble complexes with various transition metal ions, even at neutral pH levels. EDTA, which is a promising candidate for improving adsorption performance, has been widely used in industry and laboratory applications due to its high sorption efficiency, selectivity, and sensitivity.<sup>11,12</sup>

Cobalt is a valuable metal that is highly important in various industrial and military applications.<sup>13</sup> It is classified as a strategic metal asset by several countries and is included in the European Union's list of 34 critical raw materials.<sup>14</sup> This highlights its scarcity as it only makes up 0.001% of the Earth's crust. Cobalt is usually obtained as a by-product of copper and nickel refining, but its importance goes beyond traditional uses. For example, it plays a crucial role in aerospace technology where it is used to create superalloys that are essential for aircraft turbine engines.<sup>15</sup> Moreover, it is a key component in cathode materials such as lithium cobalt oxide (LiCoO<sub>2</sub>)<sup>16</sup> and lithium nickel manganese cobalt oxides (LiNi<sub>x</sub>Mn<sub>y</sub>Co<sub>1−x−y</sub>O<sub>2</sub>),<sup>17</sup> which are used in lithium-ion batteries (LIBs) that power a wide range of electronic devices such as computers and communication equipment. Due to cobalt's criticality and its higher required amount (5–10% w/w) in battery applications compared to its natural availability, an efficient recovery method from waste is essential. Recycling cobalt from industrial waste streams can reduce the environmental impact of mining, conserve resources, and ensure a stable supply for the future. Furthermore, it is possible to utilize recycled metal-adsorbent complexes to develop novel materials, such as catalysts for organic pollution degradation<sup>18</sup> or electromagnetic wave absorption,<sup>19,20</sup> thereby adding value to the recycling process and contributing to environmental sustainability.

It has been suggested in the literature that chitosan beads and silica gel can be used as adsorbents to recover cobalt ions (Co<sup>2+</sup> or Co<sup>3+</sup>).<sup>21,22</sup> To improve their adsorption capability, it has been recommended that these adsorbents be modified with ligands like EDTA. Nevertheless, the adsorption efficiency of the ligand-based adsorbent still remains insufficient and poses a challenge in the field.<sup>23,24</sup> To address the issue, this study proposes using a highly porous microsphere with a hierarchical

Department of Materials Science and Engineering, National Tsing Hua University, Hsinchu 30013, Taiwan. E-mail: cc.li@mx.nthu.edu.tw

† Electronic supplementary information (ESI) available. See DOI: <https://doi.org/10.1039/d4ma00601a>

pore structure as the adsorbent. The porous microsphere has a substantial specific surface area and the presence of numerous surface functional groups. It will be functionalized with EDTA to enhance its ability to adsorb  $\text{Co}^{2+}$ . In this preliminary exploration, the adsorption efficiency of the EDTA-modified porous microsphere will be evaluated. Based on the analyses including adsorption isotherms, X-ray photoelectron spectroscopy (XPS), kinetic studies, and simulations utilizing density functional theory (DFT), the adsorption behavior will be explained.

## Experimental

The synthesis of poly(styrene-*co*-vinyl benzyl chloride) (PSV) and the subsequent production of PSV porous microspheres, namely @PSV, have been described in detail in our prior research.<sup>25</sup> The @PSV was cross-linked by immersing it in hot concentrated sulfuric acid (95%, Honeywell, Germany) at 120 °C for 1 h. This acid-treated product, called ac@PSV, was rinsed with deionized water multiple times and then dried. The amination process involved adding 0.1 g of ac@PSV to a mixture of 30 mL ethylenediamine (EDA; 99%, Thermo Scientific, Germany) and methanol (in a 1 : 15 ratio) and allowing the reaction to proceed under reflux at 80 °C for 7 h.<sup>26,27</sup> The resulting precipitate, called en@PSV, was washed with methanol before drying in a vacuum oven at 30 °C for at least 24 h. For grafting with ethylenediaminetetraacetic acid (EDTA), 0.1 g of en@PSV was mixed with 0.5 g of ethylenediaminetetraacetic dianhydride (EDTA-dianhydride; ≥98.0%, Aladdin, China) in 120 mL *N,N*-dimethylacetamide (DMAc; 99.5%, Echo, Taiwan) and subjected to a reaction under reflux at 75 °C for 20 h.<sup>28</sup> After the reaction, the resulting product, EDTA@PSV, was washed with DMAc, a saturated aqueous solution of sodium bicarbonate (99.5%, Showa, Japan), and several rounds of deionized water before final drying in a vacuum oven at 55 °C.

In the adsorption experiment, the aqueous solution of cobalt sulfate heptahydrate ( $\text{CoSO}_4 \cdot 7\text{H}_2\text{O}$ ; 99%, Showa, Japan) was used to model the  $\text{Co}^{2+}$  in wastewater. Firstly,  $\text{CoSO}_4 \cdot 7\text{H}_2\text{O}$  was dissolved in water to create standard solutions with various  $\text{Co}^{2+}$  concentrations ( $[\text{Co}^{2+}]$ ) of 200, 300, 600, 800, 1000, and 1200  $\text{mg L}^{-1}$ , and the pH of the aqueous solution was fixed at 6. A calibration curve was created by measuring the absorbance peak intensity of the aqueous solution in the visible light range (wavelength: 350–800 nm) using a UV-Vis spectrometer (U-3010, Hitachi, Japan). In the isothermal adsorption test, various 10 mL aqueous solutions with different  $[\text{Co}^{2+}]$  were prepared at a fixed pH of 6. Then, 20 mg of EDTA@PSV was added, and the mixture was stirred at 25 °C for 24 h. After that, EDTA@PSV was separated, and the concentration of non-adsorbed  $\text{Co}^{2+}$  in the filtrate was determined using UV-Vis. The amount of  $\text{Co}^{2+}$  adsorbed was calculated based on mass balance. In an adsorption kinetic test, a 10 mL aqueous solution with a fixed  $[\text{Co}^{2+}]$  of 1000  $\text{mg L}^{-1}$  was prepared, with pH fixed at 6. 20 mg of EDTA@PSV was added, and the mixture was kept at 25 °C for different time durations. The EDTA@PSV was then separated,

and the non-adsorbed  $[\text{Co}^{2+}]$  in the filtrate and the adsorbed  $[\text{Co}^{2+}]$  onto EDTA@PSV was determined *via* UV-Vis adsorption measurements.

The morphology and composition of the @PSV were analyzed using field-emission scanning electron microscopy (FE-SEM; SU8010, Hitachi, Japan) and an energy-dispersive X-ray spectrometer (EDS; EMAX, Horiba, Japan). Pore size was measured by a mercury porosimeter (Autopore IV 9520, Micromeritics Instrument Co., USA). The surface area was measured using the gas adsorption method (ASAP 2020, Micromeritics Instrument Co., USA). Surface chemistry of various porous microspheres was characterized using Fourier-transform infrared spectroscopy (FT-IR; Vertex 80v, Bruker, Germany) and XPS (PHI 5000 Versaprobe II, ULVAC-PHI, Japan). Notably, all samples were stored in a nitrogen desiccator prior to analysis, and the FT-IR spectrometer was continuously purged with  $\text{N}_2$  gas during measurements. Zeta potential was assessed using the electroacoustic method (ZetaProbe, Colloidal Dynamics Inc., North Attleborough, MA, USA), and a contact angle test (FTA-1000B, First Ten Angstroms, USA) was also conducted. To understand how EDTA@PSV interacts with  $\text{Co}^{2+}$ , we carried out a simulation based on the DFT method using the DMol<sup>3</sup> module within the Materials Studio 2020 software package. The specific parameters for the numerical calculations are listed in Table S1 (ESI<sup>†</sup>).

## Results and discussion

The image displayed in Fig. 1a illustrates the morphology of the synthesized @PSV, with particle size varying from 5 to 20  $\mu\text{m}$ . Each microsphere has evenly distributed pores throughout its entire volume, as seen in the magnified image in Fig. 1b. The pores are present in different sizes, as shown in Fig. 1c, with an average large pore size of 3  $\mu\text{m}$ , medium pore size of 300 nm, and small pore size of 3 nm. The @PSV has a high porosity of 90%<sup>25</sup> and a high surface area of 665  $\text{m}^2 \text{g}^{-1}$  (Fig. S1, ESI<sup>†</sup>).

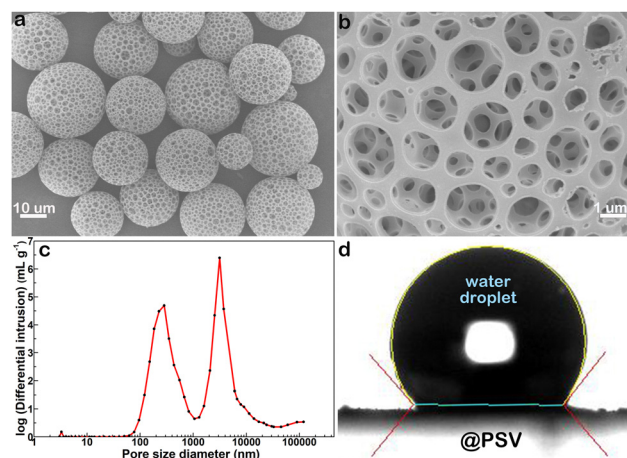


Fig. 1 (a) and (b) SEM images of @PSV with small (a) and large (b) magnifications. (c) Size distribution of pores in @PSV. (d) Contact angle measurement for @PSV.



These characteristics, along with the hierarchical pores, make it a potential adsorbent for metal ions. However, the @PSV is hydrophobic and poorly wetted by water, as revealed in Fig. 1d, where the contact angle is greater than  $129^\circ$ . This hydrophobic feature may limit its practical use in aqueous systems. To be an effective adsorbent for recycling valuable metals or removing harmful heavy metals from industrial wastewater, the @PSV should undergo surface modification with the potential ligand EDTA to enhance its capability of attracting adsorbate.

Prior to modification with EDTA, crosslinking converted @PSV to ac@PSV, resulting in improved structural and thermal stabilities (Fig. S2, ESI†).<sup>25,29,30</sup> Next, the reaction of the ac@PSV with amine yielded en@PSV,<sup>26,27</sup> which contains  $\text{-NH}_2$  groups and is capable of reacting with EDTA-dianhydride to form EDTA@PSV.<sup>26,28</sup> The FT-IR spectra of @PSV, ac@PSV, en@PSV, and EDTA@PSV are shown in Fig. 2a, with the chemical structure of PSV displayed in the inset. For @PSV, the absorption band centered at  $3453\text{ cm}^{-1}$  is usually associated with O–H stretching, which corresponds to the hydroxyl group. The benzene ring of @PSV shows vibrations that correspond to the aromatic C–H stretch at  $3026\text{ cm}^{-1}$  and the aromatic C=C stretches at  $1600$ ,  $1498$ , and  $1450\text{ cm}^{-1}$ .<sup>31</sup> The absorptions at  $2922$  and  $2847\text{ cm}^{-1}$  are assigned to the C–H stretches. The peaks at  $1000\text{--}1200\text{ cm}^{-1}$  are assigned to the C–O stretching and may belong to the  $\text{-CH}_2\text{OH}$  or  $\text{-CH}_2\text{OC}_2\text{H}_5$  groups of @PSV. The peak at  $1268\text{ cm}^{-1}$  could correspond to the  $\text{-CH}_2\text{Cl}$  wagging, and that at  $695\text{ cm}^{-1}$  could be related to the C–Cl stretch, both of which can correlate with the benzyl chloride of @PSV.<sup>31,32</sup> In the IR absorptions of ac@PSV, there is a reduction in the intensity of the peaks related to benzyl chloride, particularly the one at  $695\text{ cm}^{-1}$ . This suggests that the crosslinking reaction may have taken place *via* the  $\text{-CH}_2\text{Cl}$  group.<sup>30</sup> Additionally, there is an emergence of peaks that correspond to the asymmetric S=O stretching of the  $\text{SO}_3$  group at  $1173$  and  $1123\text{ cm}^{-1}$  and the symmetric  $\text{SO}_3$  vibrations at

$1033$  and  $1005\text{ cm}^{-1}$ , indicating the sulfonation of @PSV.<sup>31,33</sup> Moreover, the appearance of a new peak at  $1682\text{ cm}^{-1}$  related to the carbonyl (C=O) vibration of conjugated ketones or aldehydes confirms the oxidation of some  $\text{-OH}$  groups of @PSV.

The FT-IR spectrum of en@PSV displays some similarities with the spectra of @PSV and ac@PSV. However, a new peak centered at  $1630\text{ cm}^{-1}$  appears, which should be associated with the N–H bending of a primary amine or the C=N of an imine.<sup>34</sup> The broad band centered at  $3442\text{ cm}^{-1}$  is due to the overlapping stretches of O–H and N–H. The multiple absorption peaks located between  $1039\text{ cm}^{-1}$  and  $1223\text{ cm}^{-1}$  correspond to the C–N vibrations. All these observations confirm a successful amination process. After reacting with EDTA-dianhydride, the resulting EDTA@PSV shows IR absorptions similar to en@PSV. This suggests that there might be some amine groups that remained unreacted on EDTA@PSV.

Additionally, a broad band centered around  $3000\text{ cm}^{-1}$  is observed on top of the usual C–H absorption. This band is typically attributed to the O–H stretch of a carboxylic acid group.<sup>31</sup> This finding indicates that the  $\text{-NH}$  groups from en@PSV had reacted with the EDTA-dianhydride. Based on the FT-IR characterization results, we proposed the potential reactions that took place during the syntheses of ac@PSV, en@PSV, and EDTA@PSV as outlined in Scheme 1. In Scheme 1a, the reaction with concentrated  $\text{H}_2\text{SO}_4$  not only caused PSV to crosslink but should have resulted in the sulfonation of PSV and the oxidation of the carried  $\text{-OH}$ . Additionally, apart from the amination, the ketone and aldehyde groups of ac@PSV may have undergone condensation with ethylenediamine.<sup>34,35</sup>

During the contact angle measurement, it was observed that the water-repelling nature of @PSV (Fig. 1d) changed after it was converted to ac@PSV. As demonstrated in Fig. 2b, the ac@PSV absorbs the dripping water upon contact, revealing its higher hydrophilicity with a contact angle of nearly  $0^\circ$ . After amination, en@PSV shows a different level of hydrophilicity,

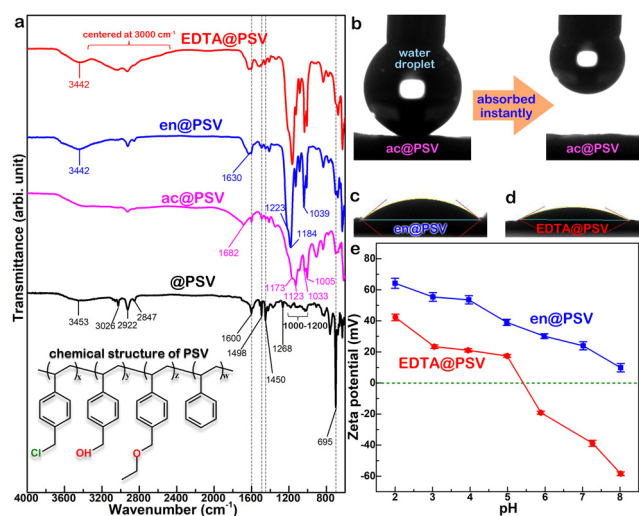
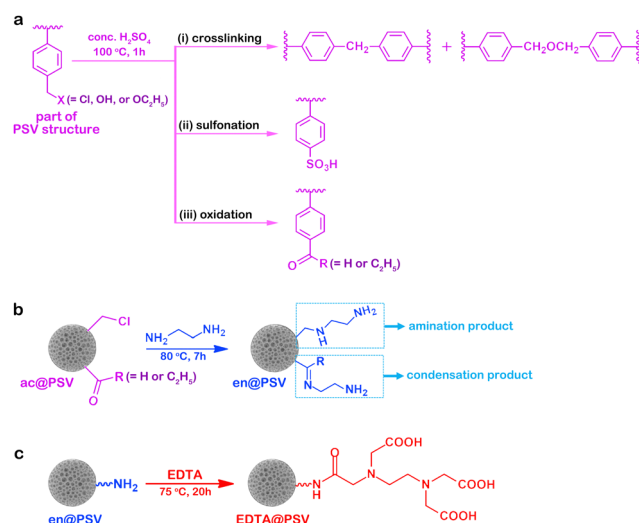


Fig. 2 (a) FT-IR spectra of various porous microspheres. Contact angle measurements for (b) ac@PSV, (c) en@PSV, and (d) EDTA@PSV. (e) Zeta potential curves of en@PSV and EDTA@PSV.



Scheme 1 Potential reactions occurring during the syntheses of (a) ac@PSV, (b) en@PSV, and (c) EDTA@PSV.

with an increased contact angle of  $40^\circ$ , as shown in Fig. 2c. EDTA@PSV shows a slight improvement in hydrophilicity compared to en@PSV, with a reduced contact angle of  $33^\circ$ , as shown in Fig. 2d. Although the contact angles of en@PSV and EDTA@PSV are similar, zeta potential measurements demonstrate that they have distinct surface chemistries, as depicted in Fig. 2e. At pH < 8, en@PSV exhibits positive zeta potentials, and there is no presence of an isoelectric point (IEP). The IEP is the pH at which the positive and negative charge densities on a particle surface are equal, resulting in zero net charge. On the other hand, EDTA@PSV has an IEP of pH 5–6, meaning that its surface is negatively charged at a pH greater than 5–6 and positively charged at other pH values. Besides, EDTA@PSV has a more negative zeta potential compared to en@PSV, making it an effective electron donor and chelator. When the pH of the solution is above 5, the negative zeta potentials of EDTA@PSV should facilitate the attraction for metal ion adsorption.

It has been previously identified through FT-IR analysis that EDTA@PSV contains several functional groups such as  $-\text{CH}_2\text{Cl}$ ,  $-\text{CH}_2\text{OH}$ ,  $-\text{CH}_2\text{OC}_2\text{H}_5$ ,  $-\text{SO}_3^-$ ,  $-\text{NH}_2$ ,  $-\text{N}-\text{C}(=\text{O})-$ , and the  $-\text{COOH}$  and  $-\text{NH}-$  of EDTA, as depicted in Fig. 3a. EDTA@PSV works as an adsorbent and the amount of  $\text{Co}^{2+}$  adsorbed has been estimated using UV-Vis spectroscopy (Fig. S3, ESI†). Fig. 3b presents the adsorption kinetics of  $\text{Co}^{2+}$  onto EDTA@PSV at pH = 6 by measuring the adsorption amount ( $q_t$ ) as a function of mixing time. It is noteworthy that  $\text{Co}^{2+}$

remains soluble in aqueous solutions up to pH 7 (Fig. S4, ESI†). A more alkaline solution will cause precipitation with  $\text{OH}^-$ , which can disrupt the adsorption experiment. In Fig. 3b, an initial concentration of  $\text{Co}^{2+}$  at  $1000 \text{ mg L}^{-1}$  was used as an example, and it can be observed that the adsorption process occurs in two stages. During the first stage, the adsorption amount increases to over  $70 \text{ mg g}^{-1}$  within an hour. In the second stage, the adsorption continues to progress, but at a slower rate until the amount reaches an equilibrium at a plateau. Both stages were analyzed using the rate equations of pseudo-first-order (Lagergren model as in eqn (1)) and pseudo-second-order (Ho and McKay model as in eqn (2)) models.<sup>26,36</sup> The pseudo-first-order kinetic model assumes that physisorption limits the adsorption rate, while the pseudo-second-order model considers chemisorption as the rate-limiting mechanism.

$$\frac{dq_t}{dt} = k_1(q_e - q_t) \quad (1)$$

$$\frac{dq_t}{dt} = k_2(q_e - q_t)^2 \quad (2)$$

where  $q_t$  and  $q_e$  are adsorption amounts at time  $t$  and at equilibrium, respectively, and  $k_1$  and  $k_2$  are the rate constant. To derive the linear forms of the pseudo-first-order and pseudo-second-order models, we integrate eqn (1) and (2) with the boundary conditions of  $q_t = 0$  at  $t = 0$  and  $q_t = q_e$  at  $t = t$ . These linear forms are given in eqn (3) and (4), respectively.

$$\ln(q_e - q_t) = \ln q_e - k_1 t \quad (3)$$

$$\frac{t}{q_t} = \frac{1}{k_2 q_e^2} + \frac{t}{q_e} \quad (4)$$

During the analysis for stage 1, we generated plots of  $\ln(q_e - q_t)$  vs.  $t$  and  $t/q_t$  vs.  $t$ , which are depicted in Fig. 3c and d, respectively. By utilizing the slope and intercept derived from these plots, we are able to calculate the adsorption parameters, including  $q_e$ ,  $k_1$ , and  $k_2$ . We repeated this process for stage 2 analysis and displayed the results in Fig. 3e and f. We have compiled the adsorption parameters obtained from both analyses in Table 1 for comparison. Our findings indicated that the pseudo-first-order and pseudo-second-order models were both well-suited to the adsorption process in stage 1, as demonstrated by the high  $R^2$  values. However, only the pseudo-second-order model was capable of predicting a  $q_e$  value that corresponds with the observation ( $\sim 75 \text{ mg g}^{-1}$ ) in Fig. 3b, indicating that this kinetic model is more appropriate. Furthermore, the adsorption in stage 2 was exclusively fitted by the pseudo-second-order model, which led to a reasonable  $q_e$  prediction. Thus, based on the above analysis, it is evident that the adsorption of

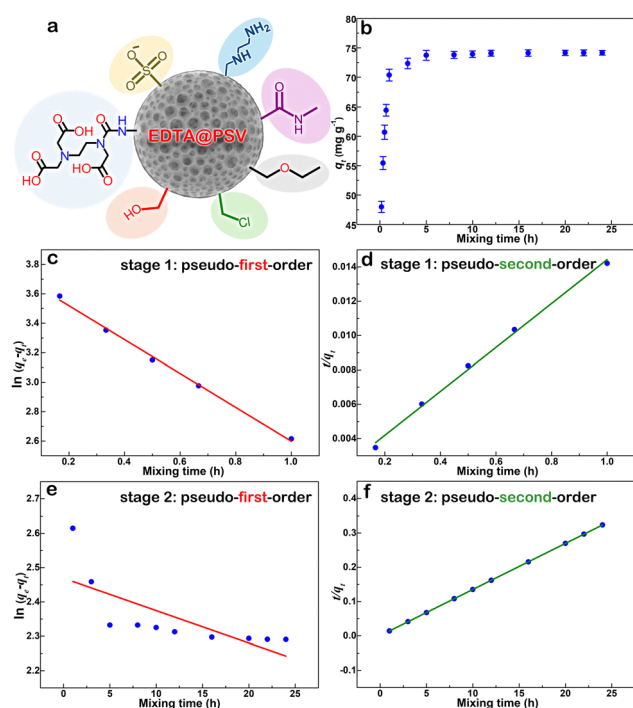


**Fig. 3** (a) A schematic showing the possible functional groups present on EDTA@PSV. (b) Adsorption amount of  $\text{Co}^{2+}$  on EDTA@PSV obtained at different mixing times at  $25^\circ\text{C}$ . (c) and (e) Pseudo-first-order and (d) and (f) pseudo-second-order kinetic plots for the  $\text{Co}^{2+}$  adsorption on EDTA@PSV at stage 1 (c) and (d) and stage 2 (e) and (f). Note: the initial concentration of  $\text{Co}^{2+}$  was  $1000 \text{ mg L}^{-1}$  at pH 6 and  $25^\circ\text{C}$ .

**Table 1** Kinetic parameters obtained for the adsorption of  $\text{Co}^{2+}$  on EDTA@PSV

Stage	Pseudo-first-order model			Pseudo-second-order model		
	$q_e$ ( $\text{mg g}^{-1}$ )	$k_1$ ( $\text{min}^{-1}$ )	$R^2$	$q_e$ ( $\text{mg g}^{-1}$ )	$k_2$ ( $\text{g mg}^{-1} \text{ min}^{-1}$ )	$R^2$
1	42.49	0.053	0.996	78.13	0.101	0.995
2	11.81	0.034	0.488	74.35	0.229	0.999





$\text{Co}^{2+}$  onto EDTA@PSV obeys the chemically pseudo-second-order kinetics.

Furthermore, the adsorption isotherm of  $\text{Co}^{2+}$  on EDTA@PSV was measured to determine the  $q_e$  of  $\text{Co}^{2+}$  at different equilibrium concentrations ( $C_e$ ) in the solution. The results are displayed in Fig. 4a<sub>1</sub>. Initially, increasing  $C_e$  leads to an increase in  $q_e$ , and then the increase gradually levels off. This suggests that the adsorption could be either monolayer adsorption on homogeneous sites or multilayer adsorption on heterogeneous sites. To confirm this, the adsorption data was analyzed using the adsorption isotherm models of Langmuir, Freundlich, Temkin, and Dubinin–Radushkevich, which are described in eqn (5)–(8),<sup>26,37</sup> respectively.

$$\frac{C_e}{q_e} = \frac{C_e}{q_m} + \frac{K_L}{q_m} \quad (5)$$

$$\ln q_e = \ln K_F + \frac{1}{n} \ln C_e \quad (6)$$

$$q_e = \frac{RT}{b_T} \ln K_T + \frac{RT}{b_T} \ln C_e \quad (7)$$

$$\ln q_e = \ln q_m - K_{DR} \varepsilon^2 \quad (8)$$

$$\varepsilon = RT \ln \left( 1 + \frac{1}{C_e} \right) \quad (9)$$

where  $K_L$  is the Langmuir binding constant related to the adsorption energy,  $K_F$  is the Freundlich adsorption constant ( $\text{mg g}^{-1}$ ),  $n$  is the heterogeneity factor that represents the bond distribution with a value within 1–10 for a favorable adsorption,  $K_T$  is Temkin isotherm equilibrium binding constant ( $\text{L g}^{-1}$ ),  $b_T$  is the heat of adsorption ( $\text{J mol}^{-1}$ ),  $K_{DR}$  is the Dubinin–Radushkevich constant ( $\text{mol}^2 \text{kJ}^{-2}$ ),  $q_m$  is the theoretical maximum adsorption capacity ( $\text{mg g}^{-1}$ ), and  $\varepsilon$  is the Polanyi potential described by eqn (9) where  $R$  is the ideal gas constant and  $T$  is the absolute temperature (K). Fig. 4a<sub>1</sub> shows that all four isotherm models are a good fit for the adsorption data. Therefore, we further assessed the linearity of the relationships between  $C_e/q_e$  and  $C_e$  using eqn (5),  $\ln(q_e)$  and  $\ln(C_e)$  using eqn (6),  $q_e$  and  $\ln(C_e)$  using eqn (7), and  $\ln(q_e)$  and  $\varepsilon^2$  using eqn (8). Linearity measures how well the adsorption conforms to a specific isotherm model. However, when we plotted  $\ln(q_e)$  against  $\ln(C_e)$ ,  $q_e$  against  $\ln(C_e)$ , and  $\ln(q_e)$  against  $\varepsilon^2$  (Fig. S5, ESI†), we obtained poor  $R^2$  values of 0.699, 0.740, and 0.735. This indicates that the adsorption of  $\text{Co}^{2+}$  on EDTA@PSV cannot be accurately described by the Freundlich, Temkin, or Dubinin–Radushkevich isotherm. In contrast, a plot of  $C_e/q_e$  against  $C_e$  shows a straight line with a high  $R^2$  value of 0.991, as shown in Fig. 4a<sub>2</sub>. This suggests that  $\text{Co}^{2+}$  adsorption on EDTA@PSV follows a monolayer Langmuir isotherm type, which occurs through chemical interaction. The good fitting result suggests that all the adsorption sites provided by

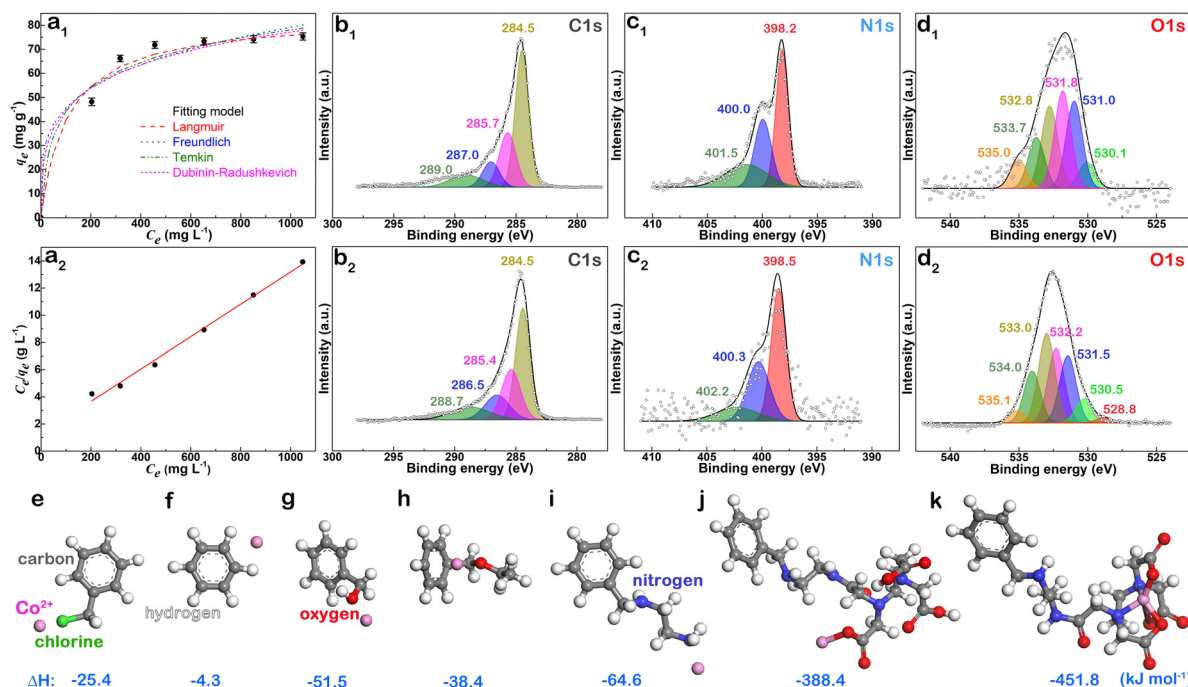


Fig. 4 (a<sub>1</sub>) Adsorption isotherm of  $\text{Co}^{2+}$  on EDTA@PSV at pH 6 and 25 °C. (a<sub>2</sub>) Langmuir isotherm linear plot for  $\text{Co}^{2+}$  adsorption on EDTA@PSV. XPS chemical state spectra of (b<sub>1</sub>) and (b<sub>2</sub>) C 1s, (c<sub>1</sub>) and (c<sub>2</sub>) N 1s, and (d<sub>1</sub>) and (d<sub>2</sub>) O 1s of EDTA@PSV before (b<sub>1</sub>), (c<sub>1</sub>) and (d<sub>1</sub>) and after (b<sub>2</sub>), (c<sub>2</sub>) and (d<sub>2</sub>)  $\text{Co}^{2+}$  adsorption. Optimized structures of different complexes formed from  $\text{Co}^{2+}$  interacting with distinct species related to the functional groups of (e) –Cl, (f) benzene, (g) –OH, (h) –O–, (i) –NH<sub>2</sub>, (j) –COOH of EDTA unit, and (k) the entire EDTA unit grafted on EDTA@PSV, with their respective formation energies indicated.



EDTA@PSV are equally attractive to adsorb  $\text{Co}^{2+}$  and do not show significant discrimination in high and low affinities. Using eqn (1),  $q_m$  can be determined from the reciprocal of the line slope, which is  $84 \text{ mg g}^{-1}$  (Table S2, ESI†). This value is higher than the values reported in the literature (usually  $30\text{--}60 \text{ mg g}^{-1}$ ),<sup>23,24</sup> which could be attributed to the large surface area, porous structure, and multiple functional groups present on the EDTA@PSV surface, facilitating the trapping of the adsorbate.

To investigate how EDTA@PSV interacts with  $\text{Co}^{2+}$ , the XPS spectra of EDTA@PSV were measured before and after  $\text{Co}^{2+}$  adsorption (Fig. S6, ESI†). The chemical state spectra of C 1s, N 1s, and O 1s are shown in Fig. 4b<sub>1</sub>, b<sub>2</sub>, c<sub>1</sub>, c<sub>2</sub>, and d<sub>1</sub>, d<sub>2</sub>, respectively. Prior to  $\text{Co}^{2+}$  adsorption, the C 1s spectrum reveals four peaks at 284.5, 285.7, 287.0, and 289.0 eV for C–C/C=C, C–N, C–O/C–Cl/O=C–N, and O=C–O, respectively, in Fig. 4b<sub>1</sub>. After  $\text{Co}^{2+}$  adsorption in Fig. 4b<sub>2</sub>, the peak corresponding to C–C/C=C remains almost unchanged at 284.5 eV, while those corresponding to C–N, C–O/C–Cl/O=C–N, and O=C–O shift to lower binding energies at 285.4, 286.5, and 288.7 eV, respectively. These changes indicate that complexes between EDTA@PSV and  $\text{Co}^{2+}$  have been formed. This suggests that the N and O atoms share their electrons with  $\text{Co}^{2+}$ , leading to an increase in electron density at their adjacent C atoms.<sup>38</sup> As a result, the binding energy of the carbons is reduced. In Fig. 4c<sub>1</sub> of the N 1s spectrum, the EDTA@PSV displays three peaks at 398.2, 400.0, and 401.5 eV. These peaks correspond to the C–N, –NH<sub>2</sub>, and O=C–N(H)– species, respectively. After  $\text{Co}^{2+}$  adsorption, all three peaks shift towards higher binding energies and are now observed at 398.5, 400.3, and 402.2 eV, as shown in Fig. 4c<sub>2</sub>. This indicates that these N-containing groups act as electron donors in complex formation with  $\text{Co}^{2+}$ .

Prior to  $\text{Co}^{2+}$  adsorption, Fig. 4d<sub>1</sub> shows the O 1s spectrum of EDTA@PSV with multiple binding energies at 530.1, 531.0, 531.8, 532.8, and 533.7 eV. These peaks represent the O atoms in  $\text{SO}_3^-$ , O=C/O=S, C–OH, C–O–C, and O–S, respectively.<sup>33,39</sup> The peak at 535.0 eV is more related to the sodium Auger peak (Na KLL). After the adsorption of  $\text{Co}^{2+}$ , the binding energies of almost all O atoms have shifted to higher values, indicating that these O atoms share their lone pair electrons with  $\text{Co}^{2+}$ . This results in a decrease in electron density, leading to an increase in the binding energy. Additionally, a new peak appears at 528.8 eV, corresponding to the binding energy of O–Co.<sup>40</sup> This indicates that a chemical bond is formed between  $\text{Co}^{2+}$  and the –OH of the hydroxyl or carboxylic acid group. We also observed a simultaneous decrease in the relative peak intensities of O=C/O=S and C–OH to  $\text{SO}_3$ , suggesting that the functional group that forms a chemical bond with  $\text{Co}^{2+}$  is the carboxylic acid rather than the hydroxyl group. In other words, the –COOH of the EDTA unit not only forms a complex but also chemically bonds with  $\text{Co}^{2+}$ .

The XPS analysis revealed that the N- and O-containing groups have a tendency to interact with  $\text{Co}^{2+}$ , but we need to note that not all of these groups are part of the EDTA unit. That is, other functional groups aside from EDTA may also exhibit interactions with  $\text{Co}^{2+}$ . To confirm this, we conducted

simulation calculations using DFT to determine the energy variations ( $\Delta E_{\text{ads}}$ ) of these species before and after  $\text{Co}^{2+}$  interaction. We simplified the calculations by modeling the functional groups present on EDTA@PSV with those shown in Fig. 4e–k. With the exception of the benzene ring (Fig. 4f) and the EDTA-grafted unit (Fig. 4j and k), other species exhibit  $\Delta E_{\text{ads}}$  in the range of  $-25$  to  $-65 \text{ kJ mol}^{-1}$ , which is similar to the heat energy ( $-40$  to  $-50 \text{ kJ mol}^{-1}$ ) released from physical adsorptions.<sup>41</sup> The small value of  $\Delta E_{\text{ads}}$  in Fig. 4f indicates that there is negligible interaction between the  $\pi$  electrons of the benzene ring and  $\text{Co}^{2+}$ . The high values of  $\Delta E_{\text{ads}}$  obtained in Fig. 4j ( $-388.4 \text{ kJ mol}^{-1}$ ) (Fig. S7, ESI†) and Fig. 4k ( $-451.8 \text{ kJ mol}^{-1}$ ) suggest that the EDTA unit forms a complex with  $\text{Co}^{2+}$  and uses its –COOH to bond with it. These values are comparable to the amount of energy released during chemical bond formation. Therefore, they are a primary mechanism responsible for the chemisorption of  $\text{Co}^{2+}$  onto EDTA@PSV as determined by the earlier adsorption analyses. Additionally, the DFT results suggest that other functional groups, aside from EDTA, also contribute to the chemical affinity of EDTA@PSV towards  $\text{Co}^{2+}$  adsorption.

## Conclusions

A new adsorbent material named EDTA@PSV has been created by modifying a hierarchical porous microsphere with an EDTA functional unit. This material demonstrates excellent adsorption properties for  $\text{Co}^{2+}$  ions when used in an aqueous environment. The original porous microsphere is hydrophobic, but after the introduction of EDTA, it became hydrophilic with a small contact angle of  $33^\circ$ . This change in surface properties makes it an ideal material for extracting valuable metal ions from an aqueous system. Furthermore, the EDTA@PSV carries a negative charge when the pH is greater than 5, which can be advantageous for attracting cationic metal ions. Most importantly, the EDTA@PSV contains various functional groups that involve N and O, such as –OH, –NH<sub>2</sub>, –N–C(=O)–. These polar functional groups are thermodynamically favorable to interact with  $\text{Co}^{2+}$  according to the DFT simulation results. In XPS characterizations, it was discovered that EDTA@PSV exhibits an electron-donation behavior during  $\text{Co}^{2+}$  adsorption. This means that the polar groups in EDTA@PSV increase their chemical affinity for  $\text{Co}^{2+}$  adsorption. Kinetic adsorption analyses showed that  $\text{Co}^{2+}$  adsorbed onto EDTA@PSV through a pseudo-second-order model, indicating a major chemisorption behavior. This conclusion was further confirmed by the adsorption isotherm measurement, which demonstrated that the  $\text{Co}^{2+}$  adsorption on EDTA@PSV was better described by the chemisorption-based monolayer Langmuir model, rather than the Freundlich, Temkin, or Dubinin–Radushkevich model. It is worth noting that the use of EDTA@PSV resulted in a high adsorption capacity of  $84 \text{ mg g}^{-1}$  for  $\text{Co}^{2+}$ . This remarkable adsorption capability can be attributed to the unique features of EDTA@PSV, such as its large surface area, porous structure, negative surface charge, and good affinity of the multiple



functional groups for  $\text{Co}^{2+}$ . Given its excellent adsorption capacity, further investigations will be conducted to study its adsorption potentials and selectivity for other metal ions in the future.

## Author contributions

Chia-Chen Li: conceptualization, writing – original draft, writing – review and editing, supervision, project administration. Mao-Hsuan Peng: investigation, methodology, validation.

## Data availability

The data supporting this article have been included as part of the ESI.†

## Conflicts of interest

There are no conflicts to declare.

## Acknowledgements

The authors are grateful for the financial support from the Industrial Technology Research Institute under the grant of 112A7042J4.

## Notes and references

- X. X. Peng, Y. S. Jiang, Z. G. Chen, A. I. Osman, M. Farghali, D. W. Rooney and P.-S. Yap, *Environ. Chem.*, 2023, **21**, 765–801.
- W. Y. Zhang, L. Y. Zhao, M. G. Xue, X. H. Duan, C. H. Feng and J. P. Zhu, *J. Cleaner Prod.*, 2023, **396**, 136455.
- X. C. Peng, Y. Su, H. J. Guo and J. Guo, *Fuel*, 2024, **367**, 131202.
- H. A. Petersen, T. H. T. Myren, S. J. O'Sullivan and O. R. Luca, *Mater. Adv.*, 2021, **2**, 1113–1138.
- T. Dutta, T. Kim, K. Vellingiri, D. C. W. Tsang, J. R. Shon, K. H. Kim and S. Kumar, *Chem. Eng. J.*, 2019, **364**, 514–529.
- A. Islam, S. H. Teo, Y. H. Taufiq-Yap, C. H. Ng, D. V. N. Vo, M. L. Ibrahim, M. M. Hasan, M. A. R. Khan, A. S. Nur and M. R. Awual, *Resour., Conserv. Recycl.*, 2021, **175**, 105849.
- Y. L. Wu, D. Lan, J. W. Ren and S. J. Zhang, *Mater. Today Phys.*, 2023, **36**, 101178.
- F. Amalina, A. S. A. Razak, S. Krishnan, A. W. Zularisam and M. Nasrullah, *Cleaner Waste Syst.*, 2022, **3**, 100051.
- K. Zhang, Z. W. Dai, W. L. Zhang, Q. Gao, Y. Dai, F. Xia and X. Zhang, *Coord. Chem. Rev.*, 2021, **434**, 213809.
- L. Q. Liang, J. H. Wang and Y. X. Zhang, *Microporous Mesoporous Mater.*, 2023, **347**, 112344.
- X. C. Chen, C. C. Yao, A. Wang, Z. D. Zhang, L. Z. Chen, J. Y. Zhang, X.-H. Liu and H.-B. Li, *J. Hazard. Mater.*, 2023, **444**, 130416.
- X. D. Cui, J. K. Zhang, Y. W. Sun, F. B. Yan, J. F. Zhao, D. D. He, Y. S. Pan, L. Yuan, Y. J. Zhai and G. Z. Hu, *Poult. Sci.*, 2023, **102**, 102346.
- C. A. Emond, V. B. Vergara, E. D. Lombardini, S. R. Mog and J. F. Kalinich, *Int. J. Toxicol.*, 2015, **34**, 44–54.
- S. E. Zhang, J. E. Bourdeau, G. T. Nwaila and Y. Ghorbani, *Resour. Policy*, 2023, **86**, 104247.
- G. Prashar, K. Thakur, S. Singh, P. Singh and V. K. Srivastava, *Superalloys for high-temperature applications: An overview*, in AIP Conference Proceedings, 2024, 2986, AIP Publishing.
- L. L. Wang, B. B. Chen, J. Ma, G. L. Cui and L. Q. Chen, *Chem. Soc. Rev.*, 2018, **47**, 6505–6602.
- B. B. Chu, Y. J. Guo, J. L. Shi, Y. X. Yin, T. Huang, H. Su, A. Yu, Y. G. Guo and Y. Li, *J. Power Sources*, 2022, **544**, 231873.
- S. Bo, J. Luo, Q. An, X. Zhao, Z. Xiao, S. Zhai and Z. Li, *J. Cleaner Prod.*, 2019, **236**, 117630.
- J. Luo, S. Bo, Y. Qin, Q. An, Z. Xiao and S. Zhai, *Int. J. Biol. Macromol.*, 2021, **166**, 1513–1525.
- Y. H. Wang and C. C. Li, *Appl. Mater. Today*, 2024, **36**, 102041.
- S. Zhuang, K. Zhu and J. Wang, *J. Cleaner Prod.*, 2021, **285**, 124911.
- E. Repo, L. Malinen, R. Koivula, R. Harjula and M. Sillanpää, *J. Hazard. Mater.*, 2011, **187**, 122–132.
- F. H. Wang, P. Wu, L. Shu, D. Huang and H. H. Liu, *Environ. Sci. Pollut. Res.*, 2022, **29**, 1–11.
- E. Repo, J. K. Warchol, T. A. Kurniawan and M. E. T. Sillanpää, *Chem. Eng. J.*, 2010, **161**, 73–82.
- C. C. Li, S. Yang, Y. J. Tsou, J. T. Lee and C. J. Hsieh, *Chem. Mater.*, 2016, **28**, 6089–6095.
- O. R. U. López, H. S. Ortega, R. E. Navarro, J. L. Valenzuela-García, L. Machi and J. M. Quiroz-Castillo, *Results Mater.*, 2023, **17**, 100369.
- W. I. Harris, D. A. Keeley, D. J. Gisch, M. H. Tegen, J. A. Jagodzinski and D. C. McDonald, *U.S. Pat.*, 8273799, U.S. Patent and Trademark Office, Washington, DC, 2012.
- A. Jalil, M. H. Asim, Z. B. Akkus, M. Schoenthaler, B. Matuszczak and A. Bernkop-Schnürch, *J. Mol. Liq.*, 2019, **295**, 111649.
- T. M'Hiri, C. Catusse, R. Catusse and J. L. J. Dubry, *React. Kinet. Catal. Lett.*, 1983, **22**, 425–428.
- M. S. M. D. Silva, C. L. D. Costa, M. D. M. Pinto and E. R. Lachter, *React. Polym.*, 1995, **25**, 55–61.
- K. Nakamoto, *Infrared and Raman Characteristic Frequencies of Organic Molecules*, 1999.
- M. Wilson, R. Kore, A. W. Ritchie, R. C. Fraser, S. K. Beaumont, R. Srivastava and J. P. S. Badyal, *Colloids Surf., A*, 2018, **545**, 78–85.
- N. Joseph, K. K. M. Illam, R. V. Bhat, N. E. Veetil, A. Kaipamangalath, M. R. Varma and S. Thomas, *J. Phys. Chem. Solids*, 2020, **145**, 109527.
- S. H. Lee, S. R. Shin and D. S. Lee, *Mater. Des.*, 2019, **172**, 107774.
- E. Kolobova1, P. Mäki-Arvela, A. Pestryakov, E. Pakrieva, L. Pascual, A. Smeds, J. Rahkila, T. Sandberg, J. Peltonen and D. Y. Murzin, *Catal. Lett.*, 2019, **149**, 3432–3446.
- N. F. Al-Harby, E. F. Albahly and N. A. Mohamed, *Polymers*, 2021, **13**, 4446.
- T. Wang, Y. Y. An, J. X. Sun, H. X. Yang, Y. Y. Huang and H. L. Zheng, *Chem. Eng. J.*, 2023, **465**, 142950.



- 38 Y. Li, Y. Q. Liang, X. M. Mao and H. Li, *Chem. Eng. J.*, 2022, **438**, 135531.
- 39 Y. Gao, L. F. Yao, S. Z. Zhang, Q. Y. Yue and W. Y. Yin, *Environ. Pollut.*, 2023, **316**, 120622.
- 40 N. S. McIntyre, D. D. Johnston, L. L. Coatsworth, R. D. Davidson and J. R. Brown, *Surf. Interface Anal.*, 1990, **15**, 265–272.
- 41 J. G. Dash, *Films on solid surfaces: the physics and chemistry of physical adsorption*, Elsevier, 2012.

